MICROROBOTS

Cooperative cargo transportation by a swarm of molecular machines

M. Akter[1], J. J. Keya[1], K. Kayano[2], A. M. R. Kabir[1], D. Inoue[3], H. Hess[4], K. Sada[1,2], A. Kuzuya[5], H. Asanuma[6], A. Kakugo[1,2]*

Cooperation is a strategy that has been adopted by groups of organisms to execute complex tasks more efficiently than single entities. Cooperation increases the robustness and flexibility of the working groups and permits sharing of the workload among individuals. However, the utilization of this strategy in artificial systems at the molecular level, which could enable substantial advances in microrobotics and nanotechnology, remains highly challenging. Here, we demonstrate molecular transportation through the cooperative action of a large number of artificial molecular machines, photoresponsive DNA-conjugated microtubules driven by kinesin motor proteins. Mechanical communication via conjugated photoresponsive DNA enables these microtubules to organize into groups upon photoirradiation. The groups of transporters load and transport cargo, and cargo unloading is achieved by dissociating the groups into single microtubules. The group formation permits the loading and transport of cargoes with larger sizes and in larger numbers over long distances compared with single transporters. We also demonstrate that cargo can be collected at user-determined locations defined by ultraviolet light exposure. This work demonstrates cooperative task performance by molecular machines, which will help to construct molecular robots with advanced functionalities in the future.

INTRODUCTION

In nature, cooperation between a large number of living entities may allow the performance of tasks exceeding the capabilities of each individual entity (*1*–*5*). For example, groups of ants or even humans cooperate to carry large loads beyond any individual's capabilities. Inspired by this cooperative behavior of living organisms, swarm robotics has emerged as a new discipline that focuses on the fabrication of robots and their utilization in swarms to accomplish complex tasks (*6*–*12*). Swarming is a collective behavior in which multiple moving entities assemble into ordered structures through their mutual interactions (*13*, *14*). To date, swarms of macroscale robots have been used for various applications, such as transportation and accumulation of loads (*15*, *16*), formation of shapes (*6*, *17*), construction of complex structures (*18*), and sequential task execution (*7*). Recent technological advancements facilitate the miniaturization of robots to the micro- or nanoscale, which improves their scalability and permits the concurrent utilization of a large number of robots (*19*–*21*).

Colloidal systems composed of active crystals or polymeric gels have been promising for fabricating tiny robots that permit the operation of a dozen to a hundred swarm units at a time (*22*, *23*). When powered by the energy of magnetic fields (*24*), electric fields (*25*), or light (*26*), these swarm robots exhibit complex collective behavior in a controlled manner. On another front, self-propelled systems, driven by chemical (*27*), enzymatic (*28*), or photochemical reactions (*29*), have also been used in fabricating microscale swarm robots because of their capability of autonomous actuation. Among the enzymatic self-propelled systems, adenosine triphosphate (ATP)–fueled biological molecular machines—for example, microtubule (MT)–kinesin/dynein—have attracted considerable attention in swarm robotics by virtue of their translational motion and engineering properties (*30*–*32*). Despite these advancements, microscale robots have not been used yet as ensembles for cooperative task achievement, as envisioned by computational studies (*33*), which is crucial for the next step in swarm robotics (*12*).

In this study, we demonstrate the cooperative task accomplishment by creating swarms of biological molecular machines, MTs propelled by kinesin motors as transporters. The swarms of MTs load and deliver cargo to a designated location through association and dissociation, respectively, in response to an applied photo signal. The swarming of the kinesin-propelled MTs is regulated by using light-controlled interactions between photoresponsive DNA attached to the MTs. The swarms facilitate the transport of large numbers and large-sized cargo over long distances, which is insurmountable for the individual transporters. Because of the cooperative operation of numerous swarm units, if loading of cargo to a carrier is unsuccessful, then surrounding swarms are able to load and deliver the cargo in an efficient manner. This work offers a transport system using swarms of micrometer-sized, self-propelled robots that can deliver cargo to a designated place in an efficient and robust manner. This scheme may draw a new route to construct task-sequencing molecular swarm robots with advanced functionalities.

RESULTS

Design and construction of swarms of molecular transporters

The design and concept of cooperative cargo transportation by groups of molecular transporters are illustrated in Fig. 1 (A and B), where visible (VIS) light irradiation triggers cargo loading and transportation, and ultraviolet (UV) light irradiation performs cargo unloading. Two kinds of molecular transporters were prepared by modifying two fluorescent dye (ATTO550 and ATTO488)–labeled

[1]Faculty of Science, Hokkaido University, Sapporo, Hokkaido 060-0810, Japan. [2]Graduate School of Chemical Sciences and Engineering, Hokkaido University, Sapporo, Hokkaido 060-0810, Japan. [3]Faculty of Design, Kyushu University, Fukuoka 815-8540, Japan. [4]Department of Biomedical Engineering, Columbia University, New York, NY 10027, USA. [5]Department of Chemistry and Materials Engineering, Kansai University, Osaka 564-8680, Japan. [6]Department of Biomolecular Engineering, Graduate School of Engineering, Nagoya University, Nagoya 464-8603, Japan.
*Corresponding author. Email: kakugo@sci.hokudai.ac.jp

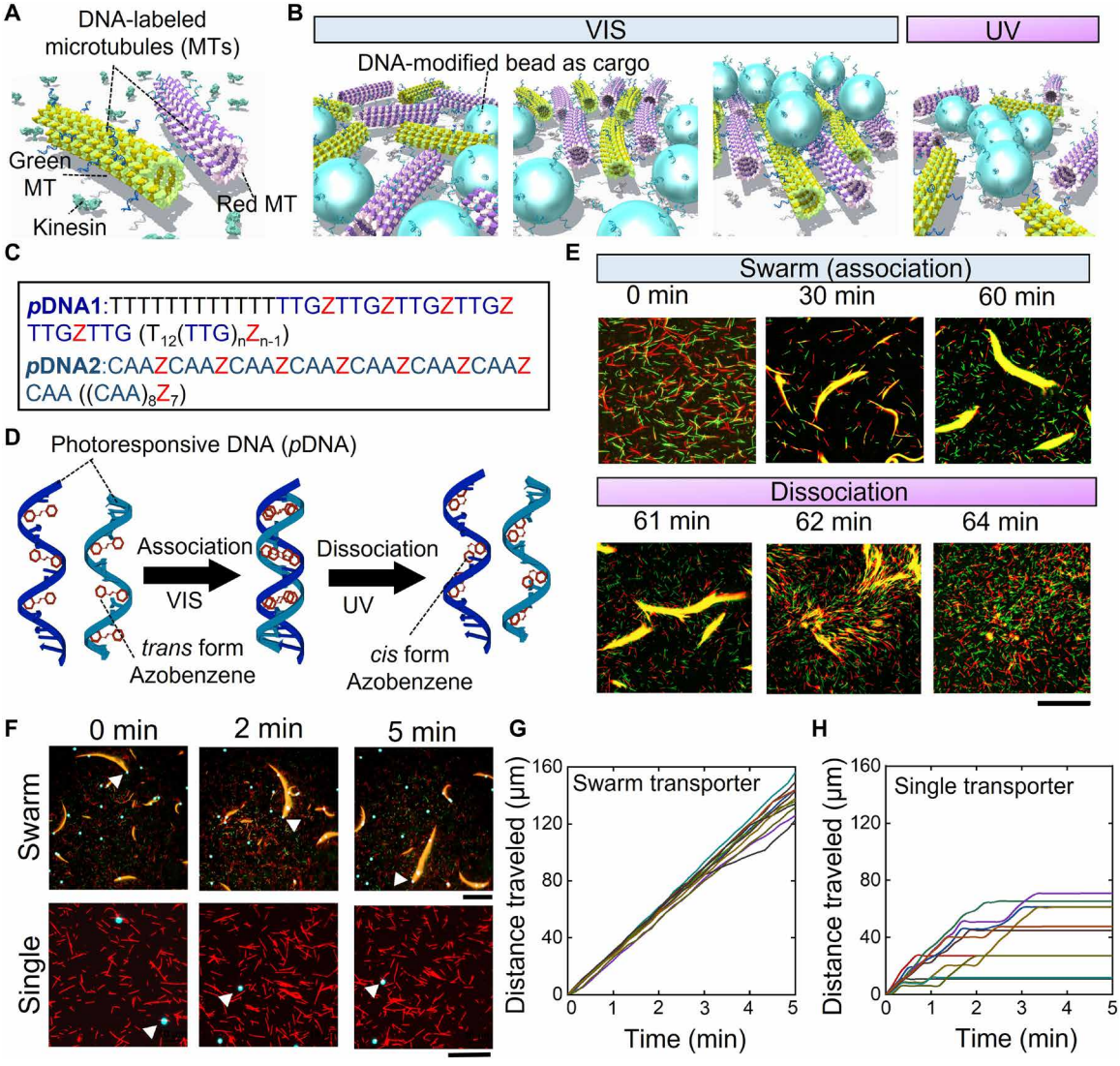

Fig. 1. Design and preparation of swarms of molecular transporters. (**A**) Schematic of the photoresponsive DNA-labeled red and green MTs gliding on a kinesin-coated surface. (**B**) Schematic illustration of the loading and transport of *p*DNA2-modified polystyrene beads as the model cargo (represented as cyan spheres) by the swarm of molecular transporters under VIS light irradiation and unloading under UV light irradiation. (**C**) Design of the photoresponsive DNA sequences to optimize molecular transporter swarming, where *n* is the number of TTG base repeats in *p*DNA1. $n = 6$ was chosen for the cargo transport experiments, and *Z* represents the azobenzene unit in the DNA strands. (**D**) Light-induced association and dissociation of azobenzene-tethered photoresponsive DNA duplexes by the cis-trans isomerization of azobenzene. (**E**) Time-lapse fluorescence microscopy images of swarm formation and the dissociation of molecular transporters under VIS (wavelength, $\lambda > 480$ nm; intensity, $I = 0.1$ mW/cm^2) and UV ($\lambda = 365$ nm and $I = 0.6$ mW/cm^2) light irradiation (scale bar, 50 μm). Molecular transporters were modified with *p*DNA1 and *p*DNA2, followed by labeling with two different fluorescent dyes with emission at 576 nm (red) and 520 nm (green) for observation under a fluorescence microscope at the same density of 40,000 mm^{-2}. The average lengths of the *p*DNA1-MTs (red MTs) and *p*DNA2-MTs (green MTs) were 6.6 ± 0.2 μm (mean ± SE) and 6.4 ± 0.3 μm, respectively. (**F**) Time-lapse fluorescence microscopy images of the loading and transportation of the cargo (diameter of 1.1 μm) by the swarm and single transporters. Scale bars, 20 μm. The white triangle shows the position of the cargo loaded by the transporter. Cargoes were modified with *p*DNA2 through a copper-free click reaction, followed by labeling with a fluorescent dye with emission at 650 nm (dark red). (**G**) Time-distance profiles of the cargo (diameter of 1.1 μm) transported by the swarms. Ten representative lines are shown for clarity. (**H**) Time-distance profiles of the cargo (diameter of 1.1 μm) transported by the single transporters. Ten representative lines are shown for clarity.

MTs with two photoresponsive single-stranded DNA, *p*DNA1 and *p*DNA2 (Fig. 1C and figs. S1 to S3), visualized as red and green, respectively. In these molecular transporters, each tubulin dimer in the MT contained one photoresponsive single-stranded DNA chain. Azobenzene, a photoresponsive molecule, was incorporated into the DNA strands to regulate their duplex formation by changing their melting temperature through cis-trans isomerization (Fig. 1D and fig. S4) (*34*).

To optimize swarm formation and cargo loading, we varied the number of TTG bases (n) and azobenzene units ($n - 1$) in each *p*DNA1 and ultimately determined them to be $n = 6$ for *p*DNA1 (table S1). Then, *p*DNA1- and *p*DNA2-modified MTs (*p*DNA1-MTs and *p*DNA2-MTs) were introduced to a flow cell and propelled by surface-adhered recombinant kinesins, consisting of the first 573 amino acid residues of human kinesin-1 with a similar velocity to that in the presence of ATP (fig. S5). Swarming of these MTs was

initiated by DNA duplex formation between the MTs, which was induced by the trans-isomerization of the azobenzene units in the single-stranded DNA under VIS light irradiation (Fig. 1E and movie S1).

The swarm grows with the VIS irradiation time in terms of length-width and association ratio (see Materials and Methods for details). It is also possible to control the growth of the swarm by changing some physicochemical parameters, such as concentration of kinesin motors, concentration of DNA (*35*), or length of DNA (fig. S6, A to C). Dissociation of the swarms was triggered by trans-to-cis isomerization upon UV light irradiation by dissociating the double-stranded DNA into single-stranded DNA (Fig. 1E and movie S1). Figure S7 shows the experimental setup for the observation of swarm formation and dissociation. The time course change in the association ratio of the *p*DNA1-MTs and *p*DNA2-MTs under VIS and UV irradiation is presented in fig. S8. The total number of single MTs in a swarm increases with the swarm size quantified as the product of swarm length and width (fig. S9).

Cooperative cargo transport by swarms of molecular transporters

The model cargo (shown in cyan) was prepared by modifying polystyrene beads (diameter = 1.1 μm) with *p*DNA2 and the fluorescent dye ATTO647 in a manner similar to that previously described (fig. S10, A and B). After 30 min of incubation for a 70% association ratio of the swarm, the cargoes were added to the flow cell to settle on the surface. The gliding swarms collided with the cargo and loaded it by duplex formation between *p*DNA1 on *p*DNA1-MT and *p*DNA2 on the cargo surface. After loading, the cargo started to move along the gliding swarms. The cargo-loading process is presented in the fluorescence microscopy images in fig. S11. The cargoes were predominantly caught by the head of the swarm and carried with a 2% decrease in velocity (fig. S12). Figure 1F (top) shows typical fluorescence microscopy images of cargo transport by the MT swarms. Movie 1 shows that the swarm-loaded cargo traveled a total distance of 1 mm without falling off.

As a control, we attempted cargo transport by gliding *p*DNA1-MTs as single transporters under conditions similar to those applied for the swarms (Fig. 1F, bottom). The same cargoes were added to the flow cell, and cargo loading and transportation were observed after the addition of ATP without any incubation. The gliding single transporters loaded the cargoes by collision and transport under VIS light irradiation, but the travel distance was much shorter than that observed with the swarms due to the cargo dropping off (fig. S13). This result was confirmed by analyzing the transport distance of the swarms and the single MTs over time (Fig. 1, G and H).

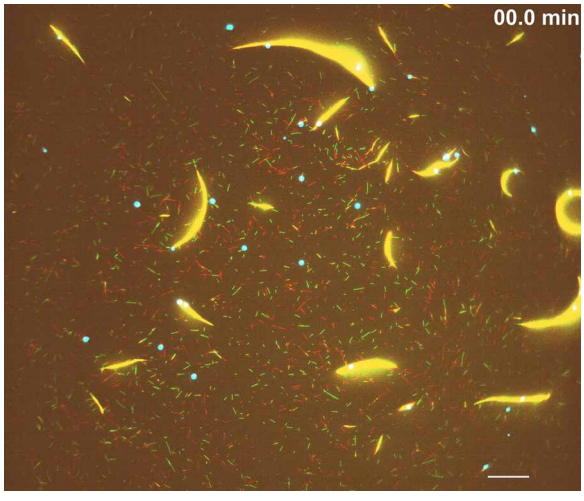

Movie 1. Cooperative task achievement by swarm transporters through loading and transporting cargo for a long distance. The movie was captured under VIS irradiation. Scale bar, 20 μm. The movie is 100 times faster than the original speed.

For swarms consisting of a few MTs, the travel distance increased roughly linearly with the number of MTs (fig. S14). Better performance of MT swarms in loading a large number of cargoes and transporting them for a longer distance could result from a larger surface area (*36*) and a larger number of binding sites on the swarms compared with the single transporters. The larger surface area of the swarms should increase the probability of collision between MTs and cargoes and reduce the probability of cargo to contact and stick to the surface. The large number of binding sites on the swarms should strengthen the interaction between cargoes and transporters and thereby reduce the probability of cargo falling off (*37*). We expect that the force that can be produced by a swarm is increased over the already substantial force produced by a single gliding MT (*38*) but that the rich dynamics predicted for rigidly coupled motors (*39*) is absent due to kinesins binding to gliding MTs with soft tails and from varied orientations (*40*).

Large cargo loading and carrying by swarms of molecular transporters

To investigate the advantages of swarms over individual transporters to carry large cargo, we investigated cargo transportation by varying the size of the cargo (polystyrene beads with diameters of 3.4, 7.2, 8.7, 20.0, and 30.0 μm). Under the same conditions, the swarms could load and transport cargoes with diameters up to 20.0 μm (Fig. 2A). In contrast, the single transporters failed to load and transport cargoes with a diameter larger than 3.4 μm (Fig. 2B, fig. S15, and Movie 2). To gain a comprehensive understanding of this difference between the swarm and single transporters, we estimated the rates of cargo attachment and detachment as a function of diameter.

Figure 2 (C and D) shows the changes in the number of cargoes loaded onto the swarm and single transporters under VIS light irradiation over time, which were curve-fitted to estimate the attachment rate (k_{on}) and detachment rate (k_{off}) (table S2) (*41*). The rates of attachment to the transporters decreased with increasing cargo size. However, the rate of attachment to the swarm transporter was much higher than that of the single transporter (Fig. 2E). Because attachment occurs due to surface collision, the ratio of the measured attachment rate k_{on} (Fig. 2F) and the collision rate between the transporter and the cargo (Z) represents the probability of duplex formation between the single-stranded DNAs of the transporter and cargo (P). The collision rate can be calculated as the product of the cargo density (D), transporter velocity (v), and effective interaction distance (g) between the transporter and cargo (see Materials and Methods for details). The effective interaction distance (g) can be inferred from the geometry of the MT-cargo interaction (Fig. 2G). The estimated duplex formation probability (P) showed good agreement with our experimental findings for 1.1- to 7.2-μm-diameter cargoes. Here, $P \approx 1$ signifies that the swarm transporters can load almost all cargoes that they encounter with diameters of 1.1 to 7.2 μm.

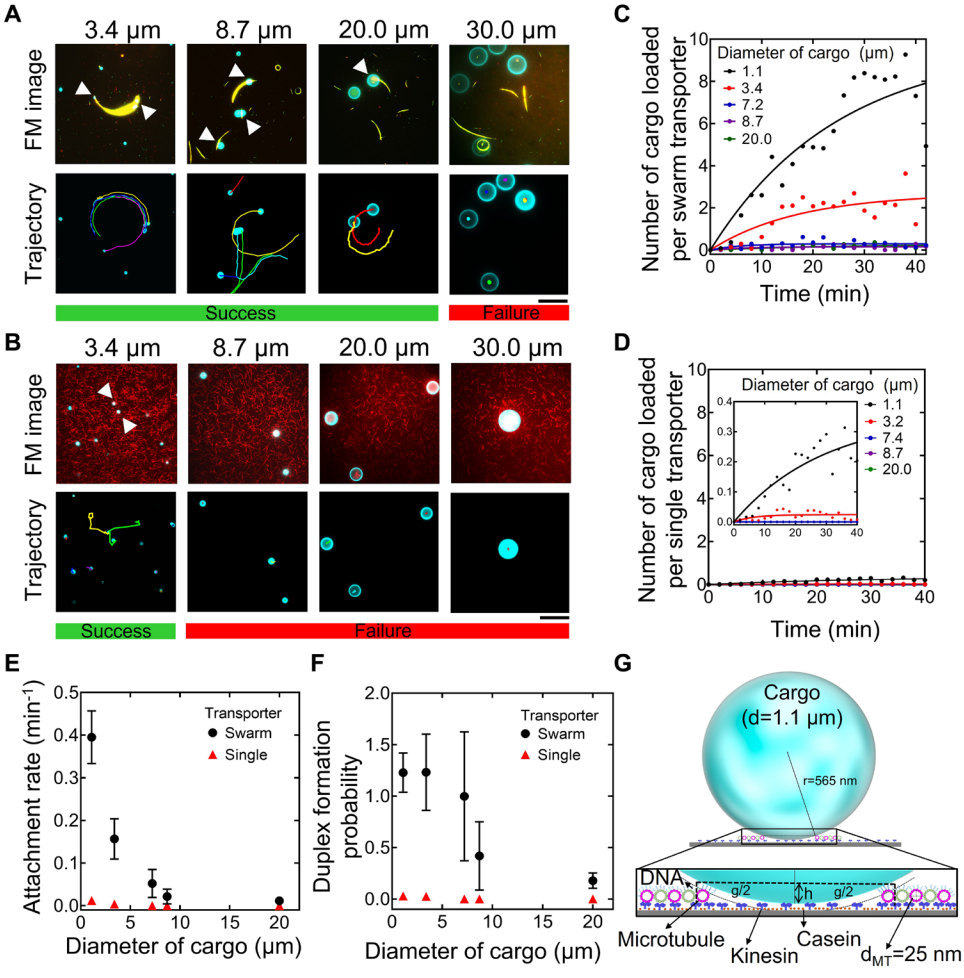

Fig. 2. Transport of large cargo by the swarm and single transporters under VIS light irradiation. (**A**) Fluorescence microscopy (FM) images of swarm transporters carrying cargoes with different diameters (3.4, 8.7, 20.0, and 30.0 μm) and the trajectories of the transported cargoes over 5 min. Scale bar, 50 μm. Green and red lines represent success and failure in cargo transportation, respectively. (**B**) FM images of the single transporters with cargoes of different diameters (1.1, 8.7, 20.0, and 30.0 μm) and the trajectories of the transported cargoes over 5 min. Scale bar, 50 μm. Green and red rectangular boxes represent success and failure in cargo transportation, respectively. (**C**) The number of cargoes loaded per swarm transporter as a function of time elapsed since cargo injection. The solid lines represent the fitting of the data according to the rate equation (see Eq. 4 in the Supplementary Materials) to obtain the attachment rates (k_{on}) and detachment rates (k_{off}). (**D**) The number of cargoes loaded per single transporter plotted as a function of time elapsed since cargo injection. The solid lines represent the fitting of the data according to the rate equation. The inset is an enlargement of the plot. (**E**) Attachment rates of the swarm and single transporters as a function of cargo diameter. Error bars: SE. (**F**) Change in the estimated duplex formation probability of DNAs on MTs in the swarm and as single transporters as a function of cargo diameter. (**G**) Approximate geometry of the MT-cargo collision to calculate the effective interaction distance between the MTs and cargo. The MTs and the cargo were placed at 17 nm (kinesin height, 17 nm) above the casein-coated glass substrate. The MTs had a radius of 12.5 nm, whereas the radius of the smallest cargo used was 565 nm (~45 times larger than that of the MTs). The effective interaction distance (g) depends on the geometries of the cargo and MT, which increases with cargo diameter.

However, when the diameters of the cargo increase further, P becomes less than 1, which signifies that the swarm transporters can still load a substantial fraction of larger cargoes. The single transporters encounter cargoes of all sizes but rarely load them. This decrease in the duplex formation probability with increasing cargo size might be accounted for by the change in the density of pDNA2 on the large cargo, the increased roughness of the cargo surface (fig. S16), or the stronger interaction between the larger cargo and the surface.

Unloading the cargo carried by the molecular transporters

The unloading of cargo from the swarm transporter or single transporter was achieved by UV light irradiation (Fig. 3, A and B). The azobenzene units in the photoresponsive DNA isomerized from the trans-to-cis conformation, which caused duplex dissociation due to the lower melting temperature of the cis form of the photoresponsive DNA. Dissociation of the swarm transporter into single MTs and cargo unloading from the transporters were observed to occur simultaneously (Fig. 3A and movie S2). The unloaded cargoes remained stationary and were no longer transported under UV light irradiation (Fig. 3, C and D).

After cargo unloading, the single MTs continued gliding with a similar velocity while dispersing in all directions on the surface and could form another swarm to again load cargo under VIS light irradiation. Unloading from the swarm transporter was completed within 5 min of UV irradiation, regardless of swarm size. Because unloading of cargo depends on the dissociation of swarms of MTs, cargoes continued to travel for some time before unloading. The time required for dissociation can be reduced by decreasing the size of the swarms, but this may undermine the advantages of transport driven by swarms (fig. S17). For the single transporter, the cargo was unloaded within 1 min of UV irradiation. The transportability of the cargo with a diameter of 1.1 μm was evaluated by the total traveled distance (s) of the cargo at a specific VIS irradiation time (t = 5 min) (see Materials and Methods) and was used to compare performance.

The mean cargo distance traveled in 5 min by the swarm and single transporters under VIS and UV light irradiation was obtained by fitting the cumulative probability distribution of the rate of total transported distance of the cargo for 5 min (fig. S18), as shown in Fig. 3E. The cargo distance traveled in 5 min by the swarm transporter was 3.4-fold higher than that of the single transporter under VIS light irradiation, and a drastic decrease was observed upon UV light irradiation for both the swarm and single transporters, which accounts for cargo unloading. Reliable dissociation of the photoresponsive DNA duplexes after UV light irradiation triggered the disassembly of swarm transporters to induce cargo unloading (Fig. 3F).

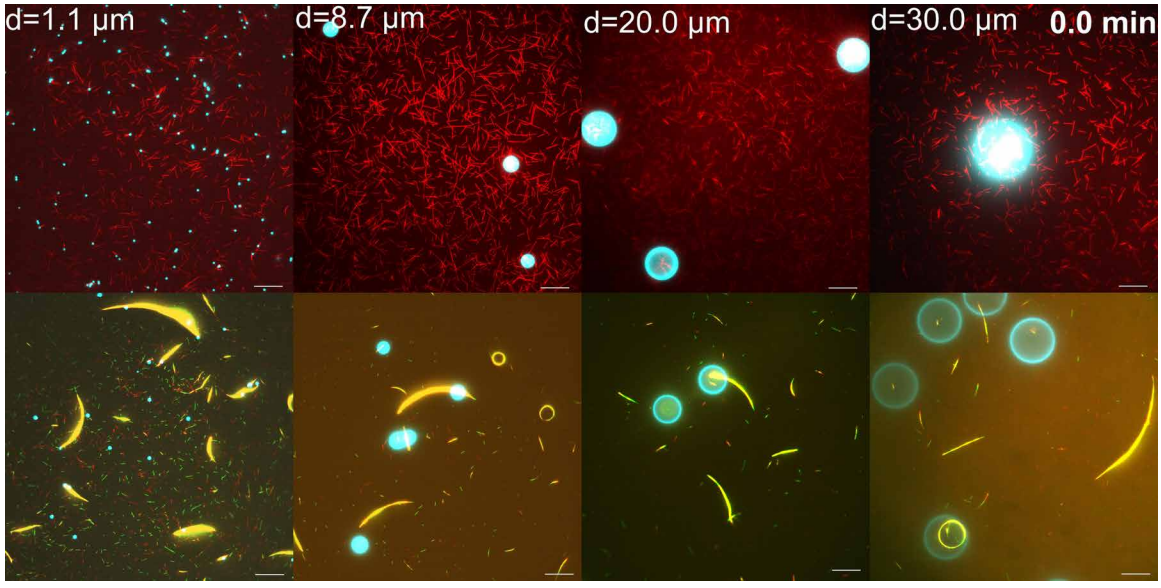

Movie 2. Different diameters of cargo loading and transporting by single and swarm transporters. Scale bars, 20 μm. The diameter of the cargo (*d*) is mentioned on the top left of each movie. The movie is 100 times faster than the original speed.

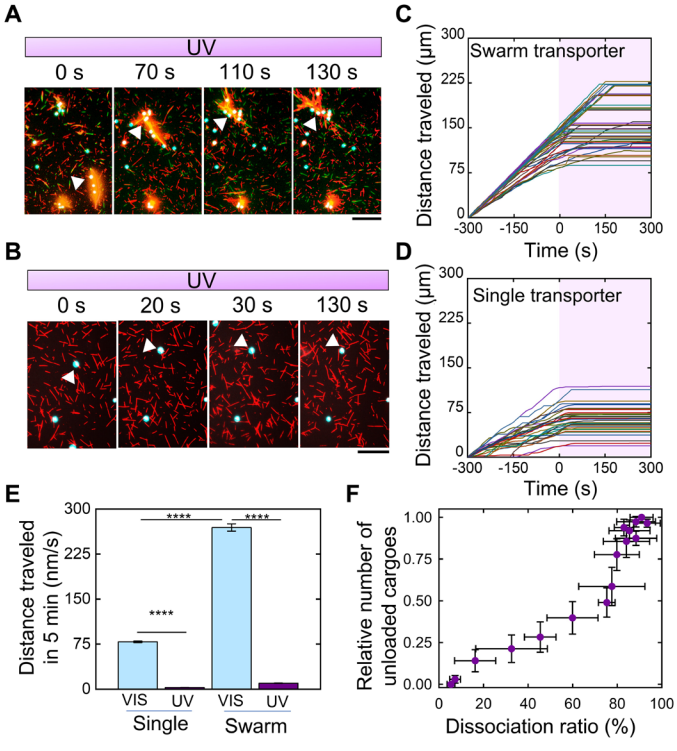

Fig. 3. Unloading of the transported cargo from the swarm and single transporters under UV light irradiation. (**A**) Time-lapse fluorescence microscopy images of cargo unloading from swarm molecular transporters under UV light irradiation ($\lambda = 365$ nm and $I = 0.6$ mW/cm^2). Scale bar, 20 μm. The white triangles show the position where the cargo is loaded onto the transporter. (**B**) Time-lapse fluorescence microscopy images of cargo unloading from single molecular transporters under UV light irradiation ($\lambda = 365$ nm and $I = 0.6$ mW/cm^2). Scale bar, 20 μm. (**C**) Cargo displacement by swarm transporters over time under VIS and UV irradiation. UV irradiation time starts at 0 s (purple area). The number of swarm transporters considered for analysis is 50. (**D**) Cargo displacement by the MT swarms over time under VIS and UV irradiation. The number of single transporters considered for analysis is 39. (**E**) Distance traveled in 5 min of cargoes loaded by the single transporters and swarm transporters under VIS and UV light. The number of analyzed events for the single and swarm transporters under VIS irradiation was 220, and under UV irradiation, the number of events for the single and swarm transporters was 100 in both cases. Statistical analysis using the Mann-Whitney *U* test confirmed a significant difference between the two datasets at $P < 0.0001$, as indicated by ****. Error bars: SE. (**F**) Change in the number of unloaded cargoes with increasing dissociation ratio of swarm transporters into single MTs under UV irradiation. Error bars: SD.

Light-controlled cargo delivery

The transportation of cargo to a designated place by a swarm transporter was attempted under external and dynamic user control. For this purpose, UV light was applied at a designated place as the cargo destination, along with VIS light, as shown in Fig. 4A. A square-shaped photomask that permitted irradiation of a 90 μm–by–90 μm area with UV light (Fig. 4B and fig. S19) was prepared, and cargo transport was carried out.

The transported cargo was unloaded at the designated place owing to the dissociation of the DNA duplex between the swarm transporter and cargo (cargo loading and swarm formation occurred simultaneously on the outside). The time lapse images in Fig. 4C illustrate that the entry of the swarm transporter carrying cargo from the VIS light region to the UV light region induced dissociation to form single MTs and caused cargo unloading (Fig. 4D and movie S3). The dissociated single MTs then returned to the VIS light region, leaving the cargo in the UV light region. Cargoes appearing outside the UV light region are deposited when swarms leave the region before the dissociation process is complete. This reduces the accuracy of swarm-based transportation.

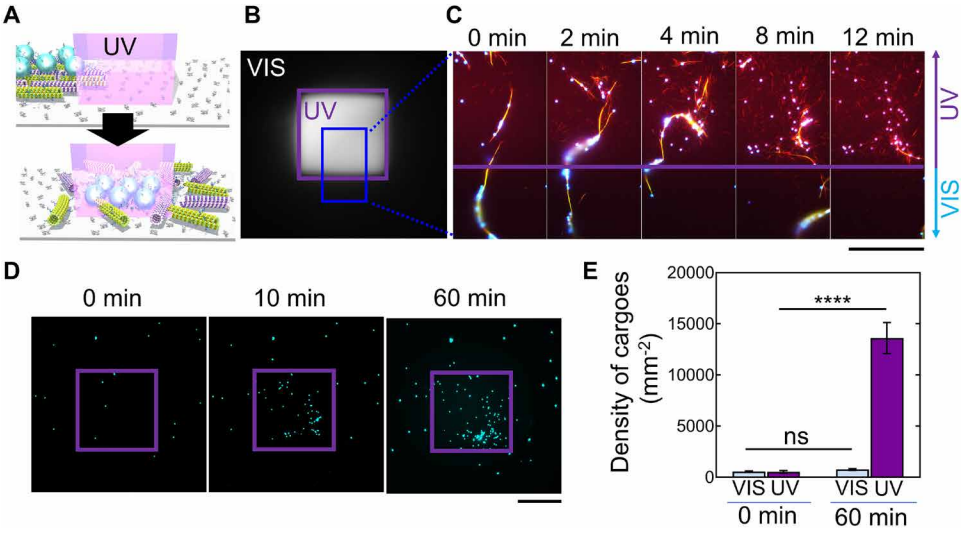

Fig. 4. Cargo unloading at a designated place. (**A**) Schematic representation showing cargo unloading by the swarm of transporters at a designated place under UV light irradiation. (**B**) Fluorescence microscopy images of the UV-irradiated place (white area) in the square purple box and VIS light–irradiated place (black area) outside of the purple box. (**C**) Time-lapse fluorescence microscopy images of cargo unloading and concentration after dissociation of swarms of molecular transporters in the UV-irradiated area. Scale bar, 50 μm. (**D**) Time-lapse fluorescence microscopy images showing the unloaded cargo in the designated UV-irradiated area. Scale bar, 50 μm. (**E**) Change in the density of the cargo over time at the designated UV-irradiated place and VIS-irradiated place. Four consecutive movies were considered for the analysis. Error bar: SD. Significant differences ($P < 0.0001$) between the two datasets are indicated by ****, and nonsignificant differences are indicated by ns (according to the Mann-Whitney *U* test).

The time course change in the number of cargoes in the UV light area is shown in Fig. 4E, indicating the accumulation of cargo in that area due to cargo unloading from swarm transporters. The rate of cargo accumulation in the UV region was much larger than that in the other region without UV light irradiation (Fig. 4E). Therefore, active cargo transport to the designated area could be achieved by controlling the photoirradiated area, indicating spatiotemporal control of cargo transport.

We also estimated the accuracy of site-specific transportation by quantifying the mean distance required to unload, which was found to be 27 ± 11 μm for a given transporter velocity (mean velocity 560 ± 30 nm/s) (fig. S20A). Therefore, the designated area should be larger than 50 μm by 50 μm. By decreasing the transporter velocity, the designated area could be reduced to 21 μm by 21 μm (fig. S20, B to D). Therefore, there is a trade-off between the velocity of transporters and the precision of cargo unloading.

For light-controlled cargo delivery by the swarm transporter, we also investigated the reversibility of cargo loading and transport under VIS light irradiation and cargo unloading under UV light irradiation. As shown in fig. S21, the unloaded cargoes from the swarm transporter after UV light irradiation could be caught and transported by another swarm transporter under VIS light irradiation. Therefore, cargo transport by swarm transporters could be controlled by changing the form of light irradiation.

DISCUSSION

In this study, we demonstrated the creation of a group of molecular machines and used their advantages over individual machines to transport large cargoes in a cooperative manner. We also describe the potential to construct such groups in the future to further amplify these cooperative behaviors. Biomolecular motor-driven molecular transportation systems have already been established, in which single entities have been used as transporters to transport cargo with diameters between 20 nm and 1 μm (*42*–*45*). In addition, loading and transporting larger cargoes over distances exceeding 50 μm remain great challenges for single filaments (*46*). The transported distance increases with the number of MTs in a swarm, which is desirable but could conceivably be achieved by repeated transport with individual MTs. Cooperation between multiple filaments could be realized when a swarm acquires the ability to move cargo that cannot be moved by individual MTs. Cargo transportation along engineered tracks has also been demonstrated by predesigning the destination with surface patterning (*47*, *48*). Cargo transport by a single entity limits transport efficiency with respect to cargo size (*37*), and the use of predefined tracks limits the directional flexibility of cargo transport. In contrast, cargo transport by swarming benefits from emergent functions, such as parallelism, robustness, and flexibility, which cannot be achieved by a single entity. High loading-transport efficiency and the ability to transport large cargo (about several hundred times larger in diameter than a single MT) are considered advantageous that can be harnessed only through cooperative tasks accomplished by swarms of transporters (*33*).

To enable cargo delivery to a designated area, the motion and delivery of the cargo should be directionally guided along predesigned tracks to well-designed delivery stations (*49*, *50*). We believe that cargo transportation that lacks such a predesigned infrastructure, as demonstrated in our work, offers flexible transportation, such as the loading and unloading of cargo in any area of interest by assigning the destination remotely through light irradiation. Introducing orthogonal controllability in the swarm system may facilitate transportation of different types of cargo at a time by the swarm transporters. Our scheme for the accumulation of cargo in a specific area may provide a framework for the efficient sorting of different types of cargo (molecules, materials, or microplastics) at different locations (*51*).

Cooperative task achievement is a strategy that has been adopted by living beings to survive. However, the mechanism by which cooperation ensures that a group functions better than the sum of the individuals at a molecular level has remained elusive. This work may offer a robust platform through which to further explore the constructive integration of complexity and emergent functions with machinery (*10*, *24*). This achievement will guide the construction of complex molecular machines with the ability to perform complex task sequencing and to overcome obstacles collectively in a working environment through the fusion of molecular computation, molecular robotics, informatics, and machine learning (*7*).

MATERIALS AND METHODS

Purification of tubulin and kinesin

Tubulin was purified from the porcine brain through two cycles of polymerization and depolymerization using a high concentration of PIPES buffer (1 M PIPES, 20 mM EGTA, and 10 mM $MgCl_2$) and then preserved in BRB80 buffer (80 mM PIPES, 1 mM EGTA, and 2 mM $MgCl_2$, pH maintained to 6.8 using KOH) (*52*). Recombinant kinesin-1 consisting of the first 573 amino acid residues of human kinesin-1 was prepared as described in the literature (*53*). Preparation of azide-labeled tubulin was performed using N_3-PEG_4-NHS following the established protocol of labeling tubulin with a fluorescent dye (*54*). The tubulin concentration was determined by measuring the absorbance at 280 nm using a UV spectrophotometer (Nanodrop 2000c spectrophotometer). ATTO550- and ATTO488-labeled tubulins (red and green) were also prepared following the same protocol.

Design and preparation of DNA sequences

Photoresponsive azobenzene tethered DNA (*p*DNA) strands were designed from melting temperature (T_m) simulation using the OligoAnalyzer tool (https://sg.idtdna.com/calc/analyzer) with a T_m between 0 and 70°C for experimental testing. *p*DNA strands were purchased from Hokkaido System Science Co. Ltd. The 5′ end of the *p*DNA was modified with dibenzocyclooctyne (DBCO). Polyacrylamide gel electrophoresis was performed to control the quality of the purchased *p*DNA. Characterization of the *p*DNA strands was carried out by LC-ESI-MS (liquid chromatography–electrospray ionization–mass spectrometry) technique. Table S1 presents the sequences of the used *p*DNAs related to experiments.

Measurement of the T_m of the *p*DNA duplex

The *p*DNA duplex (2 μM) was dissolved in 10 mM phosphate buffer (pH 7.0) with 100 mM NaCl. The *p*DNA duplex in the cis and trans state was obtained by irradiating with a high-power UV light-emitting diode lamp (SOLIS-365C, Thorlabs) having a dominant wavelength of 365 nm. Before the T_m measurement, either 365- or 450-nm light was irradiated to the *p*DNA duplex solution for 5 min. The melting curves of the duplex in the cis and trans state were obtained with a spectrophotometer (V-760 spectrophotometer, Jasco) at 260 nm in a quartz cell with a 10-mm path length (fig. S4). The heating rate was 0.5°C/min. T_m was determined from the maximum in the first derivative of the melting curve.

Preparation of MTs

MTs were polymerized from a mixture of 70 μM azide-labeled tubulin [80% (v/v)] and dye-labeled tubulin [20% (v/v)] using polymerization buffer (80 mM PIPES, 1 mM EGTA, 1 mM $MgCl_2$, and 1 mM polymerizing agent, pH ~6.8). The polymerizing agent for MTs was the nonhydrolyzable guanosine triphosphate analog guanosine-5′-[(α,β)-methyleno]triphosphate (GMPCPP). Then, the mixture was incubated at 37°C for 30 min to form GMPCPP-stabilized MTs. One microliter of 4× BRB80 buffer and 0.5 μl of 1 mM taxol were added to the MTs just after polymerization to stabilize the MTs. Copper-free click reaction was initiated by adding 3.5 μl of DBCO-conjugated *p*DNAs (200 μM) to the 5 μl of azide-MTs (56 μM), which allowed azide-alkyne cycloaddition reaction, and incubated at 37°C for 6 hours (*44*). One hundred microliters of cushion buffer (BRB80 buffer supplemented with 60% glycerol) was used to separate the MTs by centrifugation at 201,000*g* (S55A2-0156 rotor, Hitachi) for 1 hour at 37°C. After removing the supernatant, the pellet of *p*DNA-conjugated MTs was washed once with 100 μl of BRB80P (BRB80 supplemented with 1 mM taxol) and dissolved in 15 μl of BRB80P.

Measurement of the labeling ratio of *p*DNA to MTs

The *p*DNA-conjugated MTs were depolymerized to *p*DNA-conjugated tubulins keeping them on ice overnight. The absorption spectrum of the *p*DNA-conjugated tubulin dimers was measured using a spectrophotometer (NanoDrop 2000c, Thermo Fisher Scientific Inc.) and deconvoluted using the normal distribution function with Microsoft Excel (Windows Edition, Microsoft Corporation) with peaks at 260 and 280 nm. The concentrations of *p*DNA and tubulin dimers were calculated from the Beer-Lambert law using a molar extinction coefficient of tubulin dimers (115,000 liters mol^{-1} cm^{-1}) and *p*DNA (*p*DNA1 = 253,000 liters mol^{-1} cm^{-1} and *p*DNA2 = 367,800 liters mol^{-1} cm^{-1}) from which the labeling ratio was determined (fig. S3 and table S3).

Design and preparation of swarm transporters

A microfluidic channel was constructed using two glass cover slides of 40 mm by 50 mm and 18 mm by 18 mm (Matsunami Inc.) adhered together by parafilm as a spacer with a channel pattern cut out. The glass slides were plasma-treated for 3 min by a plasma etcher (SEDE-GE; Meiwafosis) to make them hydrophilic. The channel pattern (length of 22 mm and width of 1.8 mm) was designed using Brother Canvas Workspace software on the parafilm and cut with a Brother ScanNCut printer. The flow cell was prepared by setting the designed parafilm on the large cover glass and then the small slide on the top and then heating to 70°C. Five microliters of casein buffer [BRB80 buffer supplemented with casein (0.5 mg/ml)] was added to the flow cell. After incubating for 3 min, 800 nM kinesin solution was introduced into the flow cell. After washing the flow cell with 5 μl of wash buffer (BRB80 buffer supplemented with 1 mM dithiothreitol and 10 μM taxol), 5 μl of green MT (*p*DNA2-modified ATTO488-labeled MTs) solution was introduced and incubated for 2 min, followed by washing with 10 μl of wash buffer. Subsequently, 5 μl of red MT (*p*DNA1-modified ATTO550-labeled MTs) solution was introduced and incubated for 2 min, followed by washing with 10 μl of wash buffer. The motility of MTs was initiated by applying 5 μl of ATP buffer [wash buffer supplemented with 5 mM ATP, D-glucose (4.5 mg/ml), glucose oxidase (50 U/ml), catalase (50 U/ml), and 0.2% methylcellulose (w/v)]. The time of ATP addition was set as 0 hour. Soon after the addition of ATP buffer, the flow cell was placed in an inert chamber system (*55*), and the *p*DNA1-MTs and *p*DNA2-MTs were monitored using an epifluorescence microscope at room temperature (25°C). The samples were illuminated with a 100-W mercury lamp and visualized by an epifluorescence microscope (Eclipse Ti, Nikon) using an oil-coupled Nikon Plan Apo 60× objective (numerical aperture = 1.4). UV cutoff filter blocks (tetramethyl rhodamine isothiocyanate: EX 540/25, DM565, BA605/55; green fluorescent protein: EX 470/40, DM500, BA535-50; Nikon) were used in the optical path of the microscope. Images were captured using a cooled complementary metal-oxide semiconductor camera (NEO sCMOS, Andor) connected to a PC. To observe the effect of UV on the swarming of transporters, Nikon super high-pressure Hg lamp was used as a light source that passed through a UV1A filter (EX 365/10, DM400, BA390; Nikon). The beam is expanded and steered into the microscopic objective lens. UV light intensity is measured as 0.6 mW/cm^2 by a Thorlabs power meter

(PM100). The corresponding movie was captured at first under VIS light for 1 hour, taking each frame in 10-s intervals. Then, UV was irradiated to observe the dissociation of swarms into single MTs.

Measurement of the association ratio and dissociation ratio of MTs

The association ratio at a given time t was determined by counting the number of single MTs manually and dividing the number at time t by the number present initially ($t = 0$). The time-dependent association ratio, $A(t)$, of red and green MTs was determined as follows:

$$A(t) = \frac{N(0) - N(t)}{N(0)} \quad (1)$$

Here, $N(0)$ is the initial number of the single MTs, and $N(t)$ is the number of the single MTs after time t. The dissociation ratio, $R(t)$ was calculated from the ratio of the $N(t)$ and $N(0)$.

$$R(t) = \frac{N(t)}{N(0)} = 1 - A(t) \quad (2)$$

The mean association ratio and dissociation ratio were obtained from the average of four regions of interest (2500 μm^{-2}).

Cargo preparation

Amino polystyrene microbeads [5% (w/v); Spherotech Inc.] of 1.1, 3.4, 7.2, 8.7, 20.0, or 30.0 μm diameter were used as cargoes. Eighteen microliters of 20 mM N_3-PEG_4-NHS ester [dry dimethyl sulfoxide (DMSO)] and 2 μl of 20 mM ATTO647 dye (dry DMSO) were added to 20 μl of polystyrene beads, followed by the removal of supernatant from the bead suspension and washing with BRB80. The bead suspension was incubated at room temperature for 1 hour. After washing the microbeads with BRB80, microbeads were suspended in BlockAid blocking solution for 1 hour to block the hydrophobic sites of the microbeads and to reduce nonspecific adsorption. After three times washing with BRB80, 7 μl of 200 μM *p*DNA2 was mixed with the microbeads and incubated at room temperature for 24 hours. The microbeads were suspended in BRB80 to preserve for further use.

Demonstration of cargo transportation by the swarm of transporters

After the formation of swarming of transporters, 5 μl of cargoes with the desired diameter was introduced to the flow cell. Cargoes dispersed in BRB80 were diluted 30-fold with the ATP buffer before introduction to the flow cell. After incubation for 5 min, 5 μl of ATP buffer was added to the channel to wash the excess cargoes. Then, the observation was done immediately with an epifluorescence microscope. The observation process was the same as for the swarm of transporters. In addition, to observe ATTO647-labeled cargo, a bandpass filter block CY5 (EX 620/60, DM660, BA700/75) was used in the optical path of the microscope. Loading of cargoes was observed under VIS light irradiation, whereas unloading was observed under UV light irradiation. To control the cargo transportation in a designated place, UV light was irradiated through the square-shaped photomask, used in the path of UV irradiation. The UV irradiation could be controlled in any region of the observation area. The pattern structures were designed to maintain a fixed size (3 mm by 3 mm) using Brother Canvas Workspace software and cut by a Brother ScanNCut printer. That pattern permitted irradiating an area of 90 μm by 90 μm by the UV light through the 60× objective lenses. The reproducibility of each experiment related to this manuscript was checked more than 10 times.

Data analysis

The fluorescence microscopy images were analyzed by NIS-Elements AR 5.1 (Nikon) and Fiji-ImageJ 1.52J software (National Institutes of Health, USA). The velocity of the gliding MTs was measured using the ImageJ plugin "MTrackJ" (https://imagej.net/MTrackJ). The trajectories of the moving cargoes in Fig. 2 (A and B) were prepared using the FIJI-ImageJ plugin "TrackMate" (https://imagej.net/TrackMate). Statistical analysis and graphs were performed using software OriginPro Version 2019 (OriginLab, USA) and GraphPad Prism (www.graphpad.com). The D'Agostino-Pearson test, which considers the kurtosis and skewness of data, was carried out to check the normality of the data. The Mann-Whitney test or two-tailed Student's t test was used to compare two groups of data where applicable. The number of events analyzed, P value, and the name of the statistical test performed for each analysis are available in the figure legend or the caption. Error bars are also defined for each dataset in the figure caption and the supplementary raw data file.

Estimation of cargo attachment rate and duplex formation probability

The cargo attachment rate was estimated from the number of cargoes loaded to swarms or single MTs. Cargo with a wide range of diameters was added to the flow cell after swarm formation. During loading of the cargo, the swarm length was kept similar. The number of cargoes loaded per transporter (N) was recorded as a function of time. These data were modeled under the assumptions that cargo loading onto a transporter is reversible, that cargo attachment is a zero-order reaction (because of a large excess of vacant binding sites on transporters and negligible decline in surface density of cargo), and that detachment is a first-order reaction (rate proportional to sites loaded per transporter) (*41*). The dynamic process can be expressed by the following equation:

$$dN/dt = k_{on} - k_{off}N \quad (3)$$

where k_{on} is the attachment rate and k_{off} is the detachment rate. Upon solving, we get the time-dependent loading, $N(t)$, from Eq. 3. The following equation fitted the dataset for each experiment.

$$N = \frac{k_{on}}{k_{off}}[1 - \exp(-k_{off}t)] \quad (4)$$

k_{on} and k_{off} were determined from the fitted value of the equation. In the attachment process, because the cargo loading occurs only via surface collisions, k_{on} can be defined as the product of collision rate between the transporter and the cargo, Z, and the duplex formation probability between the DNAs conjugated to MT and cargo, P.

$$k_{on} = Z \times P = D \times g \times v \times P \quad (5)$$

Here, D is the cargo density and v is the gliding velocity of the transporters (single/swarm). g is the effective interaction distance, which is estimated to be 360, 600, 870, 950, and 1450 nm for diameters of 1.1, 3.4, 7.2, 8.7, and 20.0 μm cargo, respectively, based on the geometry of the kinesin bound MT and cargo. The estimates can be explained as follows: The single or swarm transporters and

cargoes are elevated 17 nm above the substrate surface (*56*). We assume that the swarm has the same effective height as a single MT as a transporter, which has a diameter of 25 nm (*57*). The height of the MT from the substrate is 42 nm (25 + 17). The lengths of *p*DNA1 and *p*DNA2 are considered to be 6.12 and 8.16 nm (1 base pair = 0.34 nm), respectively (*58*). After attachment, the length of hybridized complementary DNAs becomes 8.16 nm. The radius of MT increases from 12.5 to 18.6 nm upon *p*DNA1 functionalization, and the radius of the smallest cargo (diameter of 1.1 μm) increases from 565 to 573.2 nm. The center of the MT is at the vertical position of 29.5 nm (17 + 12.5), whereas the center of cargo is at a vertical position of 590.2 nm (17 + 573.2). Hence, the vertical separation between the two centers is 560.7 nm (590.2 to 29.5). The attachment distance (ad) for 1.1 μm diameter of cargo is estimated as 332.42 nm $\left(\text{ad} = \sqrt{8h\left(r - \frac{h}{2}\right)}\right)$[11], where h is 25 nm and r is the radius of cargo. The horizontal separation between the MT and cargo (d = 1.1 μm) for the effective interaction (g/2) can be calculated as ~180 nm [166.2 (ad/2) + 18.6 (MT radius) − 6.1 (*p*DNA1 length)]. The resulting values for the k_{on}, k_{off}, and P for each dataset are tabulated in table S2. Interaction between cargo and the surface became stronger with increasing size of the cargo as the mass of the size increases with the cargo size. Mass of 30.0-μm diameter of cargo (14.8 ng) is ~20,300 times higher than that of 1.1-μm diameter of cargo (7.3×10^{-4} ng).

Surface roughness observation by scanning electron microscopy

The surface roughness of *p*DNA2-modified cargo was observed with a scanning electron microscope (JEOL JSM-6010LA, Hokkaido, Japan). Before observation, the samples were gold-coated in an ion-sputtering machine (E-1010, Hitachi, Japan). During the observation, the acceleration voltage varied from 10 to 20 kV.

Measurement of cargo transportability (distance traveled in 5 min)

The cargo transportability by a swarm or single transporter is defined as the total distance traveled by the cargo (s) at a specific VIS irradiation time (t). It is different from the velocity of the transporter in which velocity is considered to measure the transported distance of the transporter per unit time. In the main text, transportability is termed as distance traveled in 5 min (T).

$$T = s\,(\text{nm})/t\,(\text{s}) \tag{6}$$

Here, travel distance is the distance traveled by the cargo just after loading to the transporter. The traveled distance (s) of the cargo was measured using the FIJI-ImageJ plugin MTrackJ (https://imagej.net/MTrackJ). All the cargoes from three consecutive movies were considered to measure the traveled distance of cargo by single and swarm transporters. The number of considered events for swarm and single transporters is 220 (for VIS irradiation). Under UV irradiation, the considered total number of cargoes is 100 for both swarm and single transporters. The traveled distance of cargo under UV irradiation was measured after 3 min of UV irradiation. The D'Agostino-Pearson test performed the normality test of the transport efficiencies. Mean transport efficiencies are determined by nonlinear least-squares fitting of the cumulative probability distribution of data to function: $\left(y = 1 - e^{\frac{x_0 - x}{t}}\right)$, where x_0 was set equal to the minimum value of the efficiencies analyzed in each case (fig. S16). The parameter decay constant, t, is the required mean transportability. Statistical analysis using the Mann-Whitney test confirmed a significant difference between the two datasets at $P < 0.0001$ indicated by ****.

SUPPLEMENTARY MATERIALS

www.science.org/doi/10.1126/scirobotics.abm0677
Figs. S1 to S21
Table S1 to S4
MDAR Reproducibility Checklist
Data file S1
Movies S1 to S3

REFERENCES AND NOTES

1. O. Feinerman, I. Pinkoviezky, A. Gelblum, E. Fonio, N. S. Gov, The physics of cooperative transport in groups of ants. *Nat. Phys.* **14**, 683–693 (2018).
2. A. Gelblum, I. Pinkoviezky, E. Fonio, A. Ghosh, N. Gov, O. Feinerman, Ant groups optimally amplify the effect of transiently informed individuals. *Nat. Commun.* **6**, 7729 (2015).
3. J. E. Niven, How honeybees break a decision-making deadlock. *Science* **335**, 43–44 (2012).
4. A. Shklarsh, A. Finkelshtein, G. Ariel, O. Kalisman, C. Ingham, E. Ben-Jacob, Collective navigation of cargo-carrying swarms. *Interface Focus* **2**, 786–798 (2012).
5. N. J. Mlot, C. A. Tovey, D. L. Hu, Fire ants self-assemble into waterproof rafts to survive floods. *Proc. Natl. Acad. Sci. U.S.A.* **108**, 7669–7673 (2011).
6. M. Rubenstein, A. Cornejo, R. Nagpal, Programmable self-assembly in a thousand-robot swarm. *Science* **345**, 6198, 795–799 (2014).
7. L. Garattoni, M. Birattari, Autonomous task sequencing in a robot swarm. *Sci. Robot.* **3**, eaat0430 (2018).
8. J. F. Boudet, J. Lintuvuori, C. Lacouture, T. Barois, A. Deblais, K. Xie, S. Cassagnere, B. Tregon, D. B. Brückner, J. C. Baret, H. Kellay, From collections of independent, mindless robots to flexible, mobile, and directional superstructures. *Sci. Robot.* **6**, eabd0272 (2021).
9. C. R. Kube, H. Zhang, Collective robotics: From social insects to robots. *Adapt. Behav.* **2**, 189–218 (1993).
10. A. M. R. Kabir, D. Inoue, A. Kakugo, Molecular swarm robots: Recent progress and future challenges. *Sci. Technol. Adv. Mater.* **21**, 323–332 (2020).
11. E. Bonabeau, M. Dorigo, D. de R. D. F. Marco, G. Theraulaz, G. Théraulaz, *Swarm Intelligence: From Natural to Artificial Systems* (Oxford Univ. Press, 1999).
12. G. Z. Yang, J. Bellingham, P. E. Dupont, P. Fischer, L. Floridi, R. Full, N. Jacobstein, V. Kumar, M. McNutt, R. Merrifield, B. J. Nelson, B. Scassellati, M. Taddeo, R. Taylor, M. Veloso, Z. L. Wang, R. Wood, The grand challenges of science robotics. *Sci. Robot.* **3**, 14 (2018).
13. H. Wang, M. Pumera, Coordinated behaviors of artificial micro/nanomachines: From mutual interactions to interactions with the environment. *Chem. Soc. Rev.* **49**, 3211–3230 (2020).
14. M. Rubenstein, A. Cabrera, J. Werfel, G. Habibi, J. McLurkin, R. Nagpal, Collective transport of complex objects by simple robots, in *Proceedings of the 2013 International Conference on Autonomous Agents and Multi-agent Systems* (International Foundation for Autonomous Agents and Multiagent Systems, 2013), pp. 47–54.
15. M. Gauci, J. Chen, W. Li, T. J. Dodd, R. Groß, Clustering objects with robots that do not compute, in *Proceedings of the 2014 International Conference on Autonomous Agents and Multi-Agent Systems*. (International Foundation for Autonomous Agents and Multiagent Systems, 2014), pp. 421–428.
16. N. Mathews, A. L. Christensen, R. O'Grady, F. Mondada, M. Dorigo, Mergeable nervous systems for robots. *Nat. Commun.* **8**, 489 (2017).
17. J. Werfel, K. Petersen, R. Nagpal, Designing collective behavior in a termite-inspired robot construction team. *Science* **343**, 754–758 (2014).
18. I. Slavkov, D. Carrillo-Zapata, N. Carranza, X. Diego, F. Jansson, J. Kaandorp, S. Hauert, J. Sharpe, Morphogenesis in robot swarms. *Sci. Robot.* **3**, eaau9178 (2018).
19. M. Dorigo, G. Theraulaz, V. Trianni, Reflections on the future of swarm robotics. *Sci. Robot.* **5**, eabe4385 (2020).
20. S. Palagi, P. Fischer, Bioinspired microrobots. *Nat. Rev. Mater.* **3**, 113–124 (2018).
21. B. VanSaders, S. C. Glotzer, Sculpting crystals one Burgers vector at a time: Toward colloidal lattice robot swarms. *Proc. Natl. Acad. Sci. U.S.A.* **118**, e2017377118 (2021).
22. W. Wang, W. Duan, S. Ahmed, A. Sen, T. E. Mallouk, From one to many: Dynamic assembly and collective behavior of self-propelled colloidal motors. *Acc. Chem. Res.* **48**, 1938–1946 (2015).

23. H. Xie, M. Sun, X. Fan, Z. Lin, W. Chen, L. Wang, L. Dong, Q. He, Reconfigurable magnetic microrobot swarm: Multimode transformation, locomotion, and manipulation. *Sci. Robot.* **4**, eaav8006 (2019).
24. J. Yan, M. Han, J. Zhang, C. Xu, E. Luijten, S. Granick, Reconfiguring active particles by electrostatic imbalance. *Nat. Mater.* **15**, 1095–1099 (2016).
25. J. Palacci, S. Sacanna, A. P. Steinberg, D. J. Pine, P. M. Chaikin, Living crystals of light-activated colloidal surfers. *Science* **339**, 936–940 (2013).
26. J. Katuri, W. E. Uspal, M. N. Popescu, S. Sánchez, Inferring non-equilibrium interactions from tracer response near confined active Janus particles. *Sci. Adv.* **7**, eabd0719 (2021).
27. A. C. Hortelao, C. Simó, M. Guix, S. Guallar-Garrido, E. Julián, D. Vilela, L. Rejc, P. Ramos-Cabrer, U. Cossío, V. Gómez-Vallejo, T. Patiño, J. Llop, S. Sánchez, Swarming behavior and in vivo monitoring of enzymatic nanomotors within the bladder. *Sci. Robot.* **6**, eabd2823 (2021).
28. B. Dai, J. Wang, Z. Xiong, X. Zhan, W. Dai, C. C. Li, S. P. Feng, J. Tang, Programmable artificial phototactic microswimmer. *Nat. Nanotechnol.* **11**, 1087–1092 (2016).
29. D. Inoue, G. Gutmann, T. Nitta, A. M. R. Kabir, A. Konagaya, K. Tokuraku, K. Sada, H. Hess, A. Kakugo, Adaptation of patterns of motile filaments under dynamic boundary conditions. *ACS Nano* **13**, 12452–12460 (2019).
30. T. Vicsek, Swarming microtubules. *Nature* **483**, 411–412 (2012).
31. G. Saper, H. Hess, Synthetic systems powered by biological molecular motors. *Chem. Rev.* **120**, 288–309 (2020).
32. J. J. Keya, R. Suzuki, A. M. R. Kabir, D. Inoue, H. Asanuma, K. Sada, H. Hess, A. Kuzuya, A. Kakugo, DNA-assisted swarm control in a biomolecular motor system. *Nat. Commun.* **9**, 453 (2018).
33. Y. Yang, M. A. Bevan, Cargo capture and transport by colloidal swarms. *Sci. Adv.* **6**, eaay7679 (2020).
34. H. Asanuma, X. G. Liang, H. Nishioka, D. Matsunaga, M. Z. Liu, M. Komiyama, Synthesis of azobenzene-tethered DNA for reversible photo-regulation of DNA functions: Hybridization and transcription. *Nat. Protoc.* **2**, 203–212 (2007).
35. J. J. Keya, A. M. R. Kabir, D. Inoue, K. Sada, H. Hess, A. Kuzuya, A. Kakugo, Control of swarming of molecular robots. *Sci. Rep.* **8**, 11756 (2018).
36. D. J. Needleman, M. A. Ojeda-Lopez, U. Raviv, H. P. Miller, L. Wilson, C. R. Safinya, Higher-order assembly of microtubules by counterions: From hexagonal bundles to living necklaces. *Proc. Natl. Acad. Sci. U.S.A.* **101**, 16099–16103 (2004).
37. C. Schmidt, V. Vogel, Molecular shuttles powered by motor proteins: Loading and unloading stations for nanocargo integrated into one device. *Lab Chip* **10**, 2195–2198 (2010).
38. V. Bormuth, A. Jannasch, M. Ander, C. M. van Kats, A. van Blaaderen, J. Howard, E. Schäffer, Optical trapping of coated microspheres. *Opt. Express* **16**, 13831–13844 (2008).
39. F. Jülicher, J. Prost, Cooperative molecular motors. *Phys. Rev. Lett.* **75**, 2618–2621 (1995).
40. H. Palacci, O. Idan, M. J. Armstrong, A. Agarwal, T. Nitta, H. Hess, Velocity fluctuations in kinesin-1 gliding motility assays originate in motor attachment geometry variations. *Langmuir* **32**, 7943–7950 (2016).
41. A. Agarwal, P. Katira, H. Hess, Millisecond curing time of a molecular adhesive causes velocity-dependent cargo-loading of molecular shuttles. *Nano Lett.* **9**, 1170–1175 (2009).
42. H. Hess, V. Vogel, Molecular shuttles based on motor proteins: Active transport in synthetic environments. *Rev. Mol. Biotechnol.* **82**, 67–85 (2001).
43. H. Hess, J. Clemmens, C. Brunner, R. Doot, S. Luna, K. H. Ernst, V. Vogel, Molecular self-assembly of "nanowires" and "nanospools" using active transport. *Nano Lett.* **5**, 629–633 (2005).
44. S. M. Früh, D. Steuerwald, U. Simon, V. Vogel, Covalent cargo loading to molecular shuttles via copper-free "click chemistry". *Biomacromolecules* **13**, 3908–3911 (2012).
45. S. Ramachandran, K. H. Ernst, G. D. Bachand, V. Vogel, H. Hess, Selective loading of kinesin-powered molecular shuttles with protein cargo and its application to biosensing. *Small* **2**, 330–334 (2006).
46. B. Nitzsche, F. Ruhnow, S. Diez, Quantum-dot-assisted characterization of microtubule rotations during cargo transport. *Nat. Nanotechnol.* **3**, 552–556 (2008).
47. S. Hiyama, R. Gojo, T. Shima, S. Takeuchi, K. Sutoh, Biomolecular-motor-based nano- or microscale particle translocations on DNA microarrays. *Nano Lett.* **9**, 2407–2413 (2009).
48. C. Brunner, C. Wahnes, V. Vogel, Cargo pick-up from engineered loading stations by kinesin driven molecular shuttles. *Lab Chip* **7**, 1263–1271 (2007).
49. M. G. L. Van den Heuvel, C. Dekker, Motor proteins at work for nanotechnology. *Science* **317**, 333–336 (2007).
50. Y. Mei, A. A. Solovev, S. Sanchez, O. G. Schmidt, Rolled-up nanotech on polymers: From basic perception to self-propelled catalytic microengines. *Chem. Soc. Rev.* **40**, 2109–2119 (2011).
51. A. J. Thubagere, W. Li, R. F. Johnson, Z. Chen, S. Doroudi, Y. L. Lee, G. Izatt, S. Wittman, N. Srinivas, D. Woods, E. Winfree, L. Qian, A cargo-sorting DNA robot. *Science* **357**, 6356 (2017).
52. M. Castoldi, A. V. Popov, Purification of brain tubulin through two cycles of polymerization–depolymerization in a high-molarity buffer. *Protein Expr. Purif.* **32**, 83–88 (2003).
53. R. B. Case, D. W. Pierce, N. Hom-booher, C. L. Hart, R. D. Vale, The directional preference of kinesin motors is specified by an element outside of the motor catalytic domain. 90, 959–966 (1997).
54. J. Peloquin, Y. Komarova, G. Borisy, Conjugation of fluorophores to tubulin. *Nat. Methods* **2**, 299–303 (2005).
55. A. M. R. Kabir, D. Inoue, A. Kakugo, A. Kamei, J. P. Gong, Prolongation of the active lifetime of a biomolecular motor for in vitro motility assay by using an inert atmosphere. *Langmuir* **27**, 13659–13668 (2011).
56. J. Kerssemakers, J. Howard, H. Hess, S. Diez, The distance that kinesin-1 holds its cargo from the microtubule surface measured by fluorescence interference contrast microscopy. *Proc. Natl. Acad. Sci. U.S.A.* **103**, 15812–15817 (2006).
57. L. A. Amos, T. S. Baker, The three-dimensional structure of tubulin protofilaments. *Nature* **279**, 607–612 (1979).
58. J. D. Watson, F. H. C. Crick, Molecular structure of nucleic acids: A structure for deoxyribose nucleic acid. *Nature* **171**, 737–738 (1953).

Acknowledgments: We acknowledge A. Konagaya, Professor, Tokyo Institute of Technology and S.R. Nasrin, Postdoctoral researcher, Hokkaido University for their valuable time and suggestion to improve our work. **Funding:** This research was supported by a project, JPNP20006, commissioned by the Future AI and Robot Technology Research and Development Project from the New Energy and Industrial Technology Development Organization (NEDO), Grant-in-Aid for Scientific Research on Innovative Areas "Molecular Engine" JP18H05423, Grant-in-Aid for Scientific Research (A) JP21H04434, Grant-in-Aid for Challenging Research (Pioneering) JP17K19211, Grant-in-Aid for Transformative Research Areas (A) JP20H05972, Grant-in-Aid for Scientific Research (C) JP21K04846, NSF Division of Materials Research 1807514, Japan Agency for Medical Research and Development 21am0401007, and Grant-in-Aid for Scientific Research (S) JP21H05025. **Author contributions:** Conceptualization: A. Kakugo; methodology: M.A., J.J.K., and K.K.; investigation: M.A.; visualization: M.A.; funding acquisition: A. Kakugo, H.H., A.M.R.K., H.A., and A. Kuzuya; project administration: M.A., A.M.R.K., K.S., and A. Kakugo; supervision: A. Kakugo; writing: M.A.; writing—review and editing: M.A., A.M.R.K., D.I., H.H., K.S., and A. Kakugo. **Competing interests:** The authors declare that they have no competing interests. **Data and materials availability:** All the data needed to evaluate the conclusions are present in the paper or the Supplementary Materials.

Submitted 21 September 2021
Accepted 23 March 2022
Published 20 April 2022
10.1126/scirobotics.abm0677

Science Robotics

Cooperative cargo transportation by a swarm of molecular machines

M. Akter, J. J. Keya, K. Kayano, A. M. R. Kabir, D. Inoue, H. Hess, K. Sada, A. Kuzuya, H. Asanuma, and A. Kakugo

Sci. Robot. **7** (65), eabm0677. DOI: 10.1126/scirobotics.abm0677

Science Robotics (ISSN 2470-9476) is published by the American Association for the Advancement of Science. 1200 New York Avenue NW, Washington, DC 20005. The title *Science Robotics* is a registered trademark of AAAS.